Abdominal Imaging

Published online: 8 May 2015

Abdom Imaging (2015) 40:2272–2280
DOI: 10.1007/s00261-015-0428-6

In vivo sodium MR imaging of the abdomen at 3T

Judy R. James,[1,2,3] Anshuman Panda,[1,2,3] Chen Lin,[2] Ulrike Dydak,[2,3] Brian M. Dale,[4] Navin Bansal[2]

[1]Department of Radiology, Mayo Clinic, 13400 E. Shea Blvd., Scottsdale, AZ 85259, USA
[2]Radiology and Imaging Sciences, Indiana University School of Medicine, Indianapolis, IN, USA
[3]School of Health Sciences, Purdue University, West Lafayette, IN, USA
[4]Siemens Medical Solutions, MR R&D, Cary, NC, USA

Abstract

Purpose: Transmembrane sodium (^{23}Na) gradient is critical for cell survival and viability and a target for the development of anti-cancer drugs and treatment as it serves as a signal transducer. The ability to integrate abdominal ^{23}Na MRI in clinical settings would be useful to non-invasively detect and diagnose a number of diseases in various organ systems. Our goal in this work was to enhance the quality of ^{23}Na MRI of the abdomen using a 3-Tesla MR scanner and a novel 8-channel phased-array dual-tuned ^{23}Na and ^{1}H transmit (Tx)/receive (Rx) coil specially designed to image a large abdomen region with relatively high SNR.

Methods: A modified GRE imaging sequence was optimized for ^{23}Na MRI to obtain the best possible combination of SNR, spatial resolution, and scan time in phantoms as well as volunteers. Tissue sodium concentration (TSC) of the whole abdomen was calculated from the inhomogeneity-corrected ^{23}Na MRI for absolute quantification. In addition, in vivo reproducibility and reliability of TSC measurements from ^{23}Na MRI was evaluated in normal volunteers.

Results: ^{23}Na axial images of the entire abdomen with a high spatial resolution (0.3 cm) and SNR (~20) in 15 min using the novel 8-channel dual-tuned ^{23}Na and ^{1}H transmit/receive coil were obtained. Quantitative analysis of the sodium images estimated a mean TSC of the liver to be 20.13 mM in healthy volunteers.

Conclusion: Our results have shown that it is feasible to obtain high-resolution ^{23}Na images using a multi-channel surface coil with good SNR in clinically acceptable scan times in clinical practice for various body applications.

Key words: Sodium—3T—Clinical—Liver—Body imaging—Total sodium concentration

Non-invasive sodium (^{23}Na) MRI has the ability to advance MR imaging beyond the routinely used ^{1}H MRI by providing information about tissue physiology and metabolism at the cellular level. In the normal baseline physiologic state, living cells in all body systems maintain a low concentration of intracellular sodium (Na_i^+) due to active transportation of sodium from the intracellular compartment into the extracellular matrix by Na^+/K^+ ATP-ase. Disturbances in the normal transmembrane Na^+ gradient are common in a number of pathologic conditions, particularly in cell death (e.g., in myocardial infarction or in tumors after various forms of therapy) [1]. The motivation of ^{23}Na MRI is based on the fact that in certain diseased states there is an increase in tissue [Na^+] due to interstitial and/or cytotoxic edema. Interstitial edema is caused by inflammation and vascular changes and results in an increased relative extracellular space, where the Na^+ concentration is ~10 times higher than the intracellular concentration. Cytotoxic edema is caused by plasma membrane disruption and improper functioning of the Na^+/K^+ pump and results in elevated [Na_i^+] [2]. ^{23}Na MRI can non-invasively detect and quantify the imbalances in tissue sodium levels, thereby providing the capability to characterize various physiologic and patho-physiologic states [2] that are not otherwise detectable using standard ^{1}H MRI.

Judy R. James, Anshuman Panda, and Navin Bansal are formerly with Radiology and Imaging Sciences, Indiana University School of Medicine and School of Health Sciences, Purdue University.

Correspondence to: Judy R. James; *email:* james.judy@mayo.edu

To date, abdominal applications of ^{23}Na MRI have been limited by its technical difficulties. These difficulties arise from the inherent biological and MR properties of the ^{23}Na nucleus. Tissue ^{23}Na MR signal is $\sim 10^{-4}$ times weaker than the ^{1}H MR signal because of its lower tissue concentration and MR sensitivity. In addition, ^{23}Na has a very short bi-exponential transverse relaxation pattern (T_{2short}: 0.5 to 5 ms and T_{2long}: 15–20 ms) which results in rapid and significant signal loss after excitation, thus making imaging data acquisition highly challenging [3]. The conventional ^{1}H MR sequences with long TE cannot be used for ^{23}Na acquisition scans. These properties of ^{23}Na translate to long imaging time, limited spatial resolution, and low signal-to-noise ratio (SNR). Some of the technical approaches for obtaining better quality ^{23}Na MRI require (1) increased main magnetic field strength, (2) efficient RF coil design, (3) pulse sequence and imaging protocol optimization, and 4) Ultra-short TE (UTE) techniques to acquire data immediately post-excitation to minimize signal loss [4].

To address the forth mentioned clinical challenges, we present sodium data obtained from a phased-array coil in this work. It must be noted that most of the previous published work in literature on ^{23}Na imaging in clinical practice has been limited to using volume coils. Our goal in this work was to enhance the quality of ^{23}Na MRI of the abdomen using a 3-Tesla MR scanner and a novel 8-channel phased-array dual-tuned ^{23}Na and ^{1}H transmit (Tx)/receive (Rx) coil specially designed to image a large abdomen region with relatively high SNR.

A gradient-recalled-echo (GRE) imaging sequence was optimized for ^{23}Na MRI to obtain the best possible combination of SNR, spatial resolution, and scan time without exceeding the US Food and Drug Administration (FDA) recommended specific absorption rate (SAR). A B_1 inhomogeneity image-based correction method was developed to correct for RF inhomogeneity produced by the phased-array coil and to calculate tissue sodium concentration (TSC) from the inhomogeneity-corrected ^{23}Na MRI. In addition, in vivo reproducibility and reliability of TSC measurements from ^{23}Na MRI was evaluated in normal volunteers.

Materials and methods

Coil design

A dual-tuned eight-channel ^{23}Na/^{1}H coil (Stark Contrast MRI Coils Research, Erlangen, Germany) was designed for ^{23}Na and ^{1}H MRI on Siemens 3T TIM Trio scanner (according to our design specifications). The coil design was adapted from the original design reported by Lanz et al. [5] The coil array consisted of two identical anterior and posterior plates (30 × 30 cm^2) as shown in Fig. 1. The anterior plate is slightly curved to fit the curvature of the human torso. Each plate consisted of one ^{23}Na Tx coil and four ^{23}Na Rx elements, with filters for proton decoupling, that covered a field of view (FOV) of 20 × 24 cm^2 The two large Tx coils provided a relatively homogenous radio-frequency (RF) excitation and deep penetration (~30 cm), and the eight Rx elements provided a high SNR. Each coil plate also consisted of a ^{1}H Tx/Rx loop arranged around the ^{23}Na Rx-arrays for ^{1}H MRI for co-registration purposes without having to use the inbuilt body coil. The ^{1}H and the ^{23}Na transmit coils on the anterior and posterior plates formed Helmholtz pairs and shared one transmit connector which helped in distributing the power to the two coils using this single connector. The transmit signal passed through a frequency filter and splitter to the respective ^{1}H and ^{23}Na transmit circuits. A common output cable aided in attaching the four independent ^{23}Na receiver channels per plate to the patient table connectors. The flexibility to use the inbuilt body coil, when the 8-channel dual-tuned ^{23}Na/^{1}H coil is plugged-in, was made possible by cable traps and detuning units. The eight ^{23}Na and two ^{1}H channels were decoupled using a number of low-noise preamplifier decouplers to minimize over all noise in the image. Additional decoupling was achieved by preamplifier decoupling used between all receiver elements. Decoupling between all elements was sufficient for the use of parallel imaging techniques and to obtain adequate SNR. The signal was phase corrected and sent to the coils through respective matching circuits. Each coil consisted of matching, blocking, and detuning circuits to ensure that the appropriate coils are active and tuned for the specific acquisition. Plugging in this coil disabled the scanner's body coil so that only the ^{1}H channel of the dual-tuned coil was used to acquire ^{1}H images [6]. The inbuilt scanner body coil was not used for transmission purposes.

Two sets of polyethylene tubes (6-mm diameter) filled with 150 mM NaCl were placed around the top and bottom ^{23}Na Rx elements covering 20 × 24 cm^2 (Fig. 1). These tubes served as fiducial markers for co-registration purposes, signal intensity normalizations, and RF inhomogeneity correction. A 43-cm long and a 2-cm diameter tube filled with 100 mM NaCl attached on the left side of the bottom plate (Fig. 1) was used as a ^{23}Na MRI signal intensity reference to calculate tissue sodium concentration. The concentration of NaCl in the reference tubes was chosen to match the in vivo loading and conductivity properties in accordance with the American College of Radiology (ACR) body phantom recommendations [7]

^{23}Na MR image acquisition optimization

A 20 L plastic carboy container filled with 50 mM NaCl was used as a phantom for pulse sequence development and protocol optimization. A modified 3D GRE imaging sequence, Volumetric Interpolated Breath Hold Examination (VIBE) [8], was used for acquiring trans-axial ^{23}Na images with the 8-channel dual-tuned ^{23}Na/^{1}H coil.

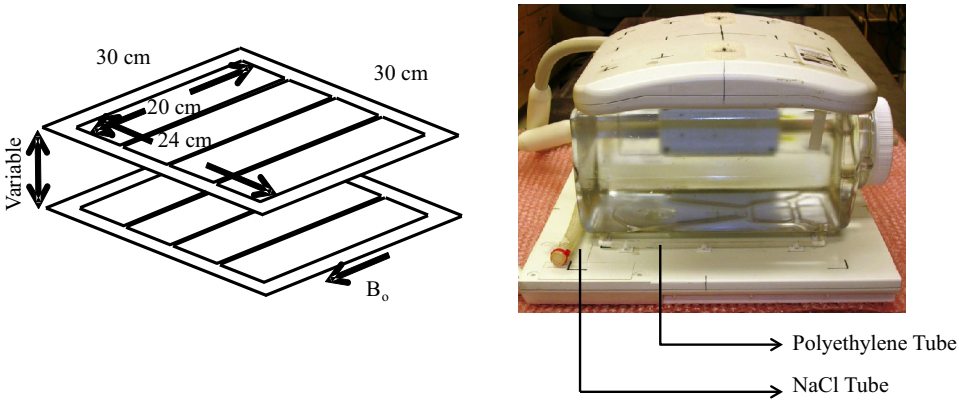

Fig. 1. Design for the 8-channel dual-tuned ^{23}Na and ^{1}H torso coil with the polyethylene and NaCl tubes used for co-registration and signal intensity reference to calculate tissue sodium concentration.

A very short echo time (TE) was used to minimize signal loss due to transverse relaxation. The short TE was achieved using asymmetric echoes (partial Fourier) combined with volumetric interpolation. The minimum allowed receiver bandwidth (BW) was used to reduce the noise level. RF transmitter was calibrated by measuring ^{23}Na SI as a function of transmitter voltage and a flip angle that matched the Ernst angle condition was used for achieving maximum SNR. Use of a short repetition time (TR) and the use of asymmetric echoes allowed collection of large number of signal averages over a reasonable time period but with lower resolution images. Elliptical acquisition was applied to further improve the SNR and to maintain the spatial resolution while reducing imaging time. The shimming of the magnet was done using the water ^{1}H signal prior to acquiring any MR images. To further improve the SNR, vendor-provided 3D field map technique followed by manual shimming was employed to achieve the optimal full width half maximum for signal over the entire volume to improve SNR.

B_1 inhomogeneity calibration curves were developed for the coil to correct for signal drop out toward the center of the image (typical drawback of all surface coils) to obtain uniform ^{23}Na images. B_1 inhomogeneity correction maps for both the top and bottom coil plates were computed individually from ^{23}Na images of a homogenous 20 L NaCl phantom. The exponentially varying signal intensity (SI) from the 3D B_1 field map for each coil plate was used to calculate calibration maps for each coil plate. The co-registered calibration maps from both the plates were then added to form a combined calibration image. The acquired ^{23}Na images from the scanner were then divided by the combined calibration image to obtain a B_1-inhomogeneity-corrected ^{23}Na image.

In vivo sodium imaging acquisition

Study population

All the MR scans were performed on a 3T scanner (Magnetom Trio: A Tim System, *Siemens*, *Erlangen*, *Germany*) after obtaining approval from the institutional review boards and written informed consent from all subjects. In vivo 3D ^{23}Na was performed on healthy volunteers (two male subjects and one female subject, age range 35–45 years). The male and female subjects were scanned 3–5 times in separate sessions.

In vivo ^{23}Na and ^{1}H MRI

The subjects were positioned supine on the bottom plate of the coil with liver positioned in the center of the coil. The curved top plate was placed at the top of the torso and aligned with the bottom plate using laser markers. No respiratory or cardiac gating was used. The top plate was free to move up and down with the subject's abdominal movement during respiration, but this movement was minimized by adding straps to hold the top plate in place. Furthermore, subjects were instructed to breathe in a short, shallow pattern instead of long, deep breaths during data acquisition. The coil was designed so that hardware performance is not degraded by slight respiratory movement of the top coil although typical breathing artifacts could not be avoided and can be observed in images. To increase the reproducibility of coil positioning, water-filled fiduciary markers were placed on both anterior and posterior coil plates around the coil circumference to be used as reference points for acquisition planning and post-processing alignment (Fig. 1). These markers on the coil surface ensured that the patient is placed reproducibly with respect to the coil at the exact same location each time. 3D trans-axial and oblique ^{23}Na images were acquired with a modified GRE pulse sequence using the following optimized parameters: TR = 12 ms, TE = 2.81 ms, number of averages = 128, BW = 130 Hz/px, flip angle = 50°, matrix size = 128 × 128, FOV = 40 × 40 cm^2, number of slices = 12, and slice thickness = 20 mm. The total acquisition time was 14.15 min.

Corresponding 3D multi-slice ^{1}H images were acquired for anatomical co-registration using the same dual-tuned ^{23}Na/^{1}H coil without moving the patient. A Half-Fourier Acquisition Single-Shot Turbo Spin-E-

cho (HASTE) pulse sequence was used with the following imaging parameters: TR = 1000 ms, TE = 105 ms, number of averages = 1, slice orientation = trans-axial, data matrix = 512 × 512, FOV = 40 × 40 cm^2, number of slices = 24, slice thickness = 8 mm, and slice gap = 2 mm. The total acquisition time was 1.25 min.

SNR in the ^{23}Na images, after applying calibration correction for coil inhomogeneity, was evaluated from the mean signal intensity obtained from region of interest (ROI) placed in a homogenous region (e.g., liver) and dividing the average liver signal with the standard deviation in the background noise in a location away from the anatomy in the frequency encoding direction.

TSC measurements

To compute TSC in the liver, SI from the liver region of ^{23}Na liver image and the SI from the reference region were acquired. Since the high-resolution ^{1}H images gave a better visualization of the liver, the liver ROI was first placed on the high-resolution ^{1}H images and then transferred to the ^{23}Na images for qualitative accuracy. TSC was calculated using the SI from the 100 mM saline reference tube (as shown in Fig. 1) and the liver tissue:

$$\mathrm{TSC} = \frac{S^{\mathrm{tiss}} \times [Na]^{\mathrm{std}}}{S^{\mathrm{std}}} \times \frac{1 - e^{-TR/T1^{\mathrm{Std}}}}{1 - e^{-TR/T1^{\mathrm{tiss}}}} \times \frac{e^{-TE/T2^{\mathrm{std}}}}{F_f \times e^{-TE/T2f^{\mathrm{tiss}}} + (1 - F_f) \times e^{-TE/T2s^{\mathrm{tiss}}}}, \quad (1)$$

where S is the signal intensity and 'std' and 'tiss' represent the SI from the 100 mM saline reference and the liver tissue, respectively. The fast relaxation fraction component of sodium (0.16) measured from experimental results was also added to the equation [9]. The sodium relaxation times used for the standard saline reference were T_1^{std} = 64 ms and T_2^{std} = 60 ms [10]. The relaxation times used for the sodium signal in the liver tissue were T_1^{tissue} = 33.8 ms, T_{2f}^{tissue} = 1.8 ms, and T_{2s}^{tissue} = 17.3 ms as reported by Bansal et al. [9].

Statistical analysis

Liver TSC values were compared to evaluate the reproducibility and the reliability between subjects. Intra- and inter-subject variability and % standard deviation (S.D.) from the mean in both measurements were examined. Statistical analysis of the imaging data values was performed by two-tailed Student's t test. A p value of ≤0.05 was used to denote statistical significance between groups for the MR imaging technique.

Results

^{23}Na images of the 50 mM phantom before and after sodium imaging parameter optimisations are shown in Fig. 2. The 8-channel dual-tuned ^{23}Na/^{1}H coil gave approximately two times better average SNR than the inbuilt body coil for proton ^{1}H images (Fig. 3). ^{23}Na human abdomen images acquired with the 8-channel ^{23}Na/^{1}H coil are shown in Fig. 4a. Corresponding ^{1}H images acquired with the same coil are also shown in Fig. 4b. The 8-channel ^{23}Na/^{1}H coil also provided better shimming compared to the body coil with both automatic 3D phase mapping technique and manual adjustments of shim currents. The ^{23}Na images of the 20 L 50 mM NaCl solution phantom, collected using the 8-channel ^{23}Na/^{1}H coil with 3D GRE imaging sequence and the optimized imaging parameters, had an average SNR of ~20. A high in-plane resolution for the ^{23}Na images was achieved using the dual-tuned coil (0.3 × 0.3 cm^2). The corresponding ^{1}H images collected for anatomical comparison had a resolution of 0.08 × 0.08 cm^2. Figure 4 shows that a large coverage of the human torso in the superior–inferior (head-foot) direction is possible with the coil while maintaining adequate SNR in both the ^{23}Na and ^{1}H images. However, a significant signal drop in the anterior–posterior direction (B_1 inhomogeneity) can be observed toward the center of each ^{23}Na slice. There was an exponential drop in the signal toward the center of the image which made the central liver region appear darker (Fig. 5). The mean signal intensity of the liver calculated near the edge of the coil plate is 196.5 compared to 116.5 in the center of the image. The drop in the signal intensity was corrected by creating 3D B_1 calibration maps from both the top and bottom coil plates separately as described in the methods section.

Figure 5 (first row) shows a representative slice from a ^{23}Na image of the 20 L phantom before and after B_1 inhomogeneity correction. A similar correction was

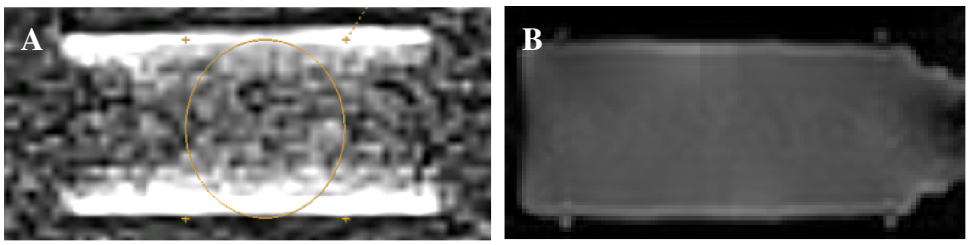

Fig. 2. ^{23}Na images of the 20 L 50 mM NaCl phantom before (**A**) and after (**B**) sodium imaging sequence parameter optimizations.

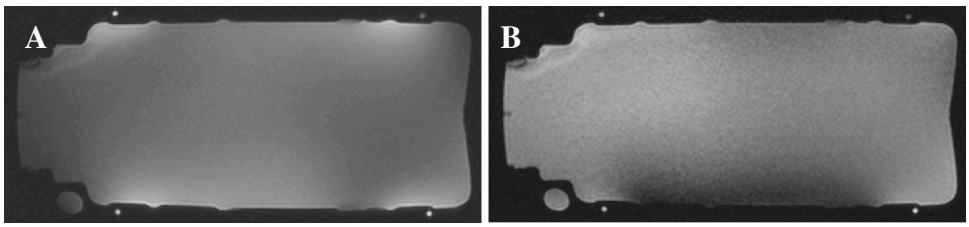

Fig. 3. Proton images of 20 L 50 mM NaCl phantom acquired with **A** dual-tuned 8-channel $^{23}Na/^{1}H$ coil and **B** inbuilt body coil for SNR comparisons.

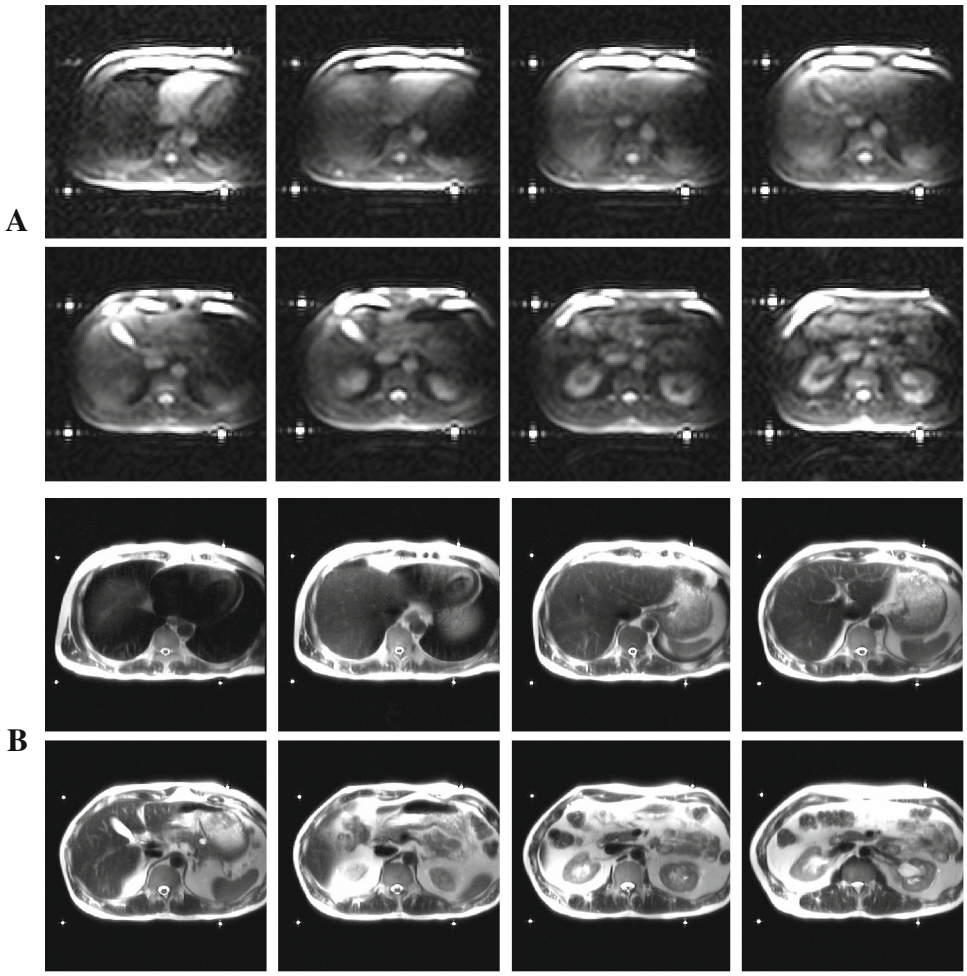

Fig. 4. Selected transaxial ^{23}Na images (**A**) and the corresponding ^{1}H image (**B**) of a healthy volunteer acquired on the 3-T MR system using the 8-channel dual-tuned $^{23}Na/^{1}H$ coil.

applied to the in vivo ^{23}Na images. Representative transaxial ^{23}Na sections of the torso before and after B_1 inhomogeneity correction and the corresponding sections from the ^{1}H images are also shown in Fig. 5 (last row). A relatively homogeneous ^{23}Na SI can be seen from the liver in the middle row. The kidneys in the last row appear hyper-intense on the ^{23}Na images due to high $[Na^+]$ in the medulla. The ^{23}Na MR images of the kidneys obtained in this study clearly show the presence of the medullary pyramids present in the peripheral part of the kidney, which can be helpful in quantifying the total sodium concentration and sodium gradients across the cortico-medullary junction in kidneys. Figure 6 shows oblique ^{23}Na and ^{1}H sections through the kidney and spine of another volunteer. The medullary pyramids present in the peripheral part of the kidney can be clearly seen in the left column. The inter-vertebral disks appear bright and the vertebral bodies appear dark in the oblique ^{23}Na image of the spine.

The quantitative analysis performed on B_1 inhomogeneity-corrected images to estimate the TSC of the liver showed that mean liver TSC was 19.8 ± 0.8 mM with

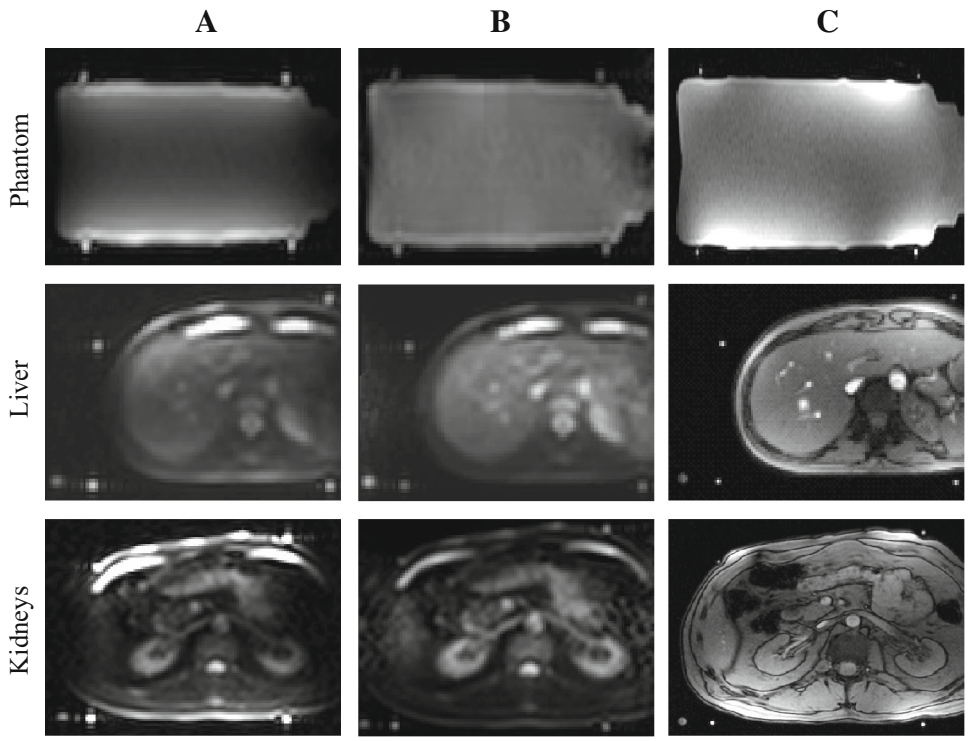

Fig. 5. Trans-axial ^{23}Na images of a 20 L NaCL phantom and in vivo liver and kidney slices before (**A**) and after (**B**) RF inhomogeneity correction and (**C**) corresponding ^{1}H slices.

4.2 % intra-subject variability for subject 1 and 20.5 ± 0.9 mM with 4.5 % variability for subject 2. The average TSC combined from both subjects was 20.1 ± 0.9 mM with a 4.4 % inter-subject variability. Two-tailed student's t test showed that the TSC values obtained from two subjects were not significantly different from each other ($p = 0.29$). Subject 3, a healthy female volunteer, had a liver TSC of 21.8 mM. A normalized z-score of 1.87 proved that the liver TSC value from the third subject showed close correlation ($p = 0.98$) to the liver TSC values measured from the male subjects at both $\alpha = 0.05$ (95% confidence) and $\alpha = 0.01$ (99% confidence) levels.

Discussion

The key biological parameters that can be measured by ^{23}Na MR are the detection of extracellular sodium concentration and quantitative TSC measurements both of which have shown promising results in various clinical indications within and outside the abdomen. A routine ^{23}Na MRI could be useful for detecting and assessing ischemic damage which results in an increase in intracellular [Na^+] [11]. It has shown to aid in the diagnosis of hepatitis- and cirrhosis-producing changes in intracellular [Na^+] and extracellular matrix structure [12] in the liver. ^{23}Na MRI has also proved useful for distinguishing between benign and malignant tumor since rapidly proliferating tumor cells are shown to have a high intracellular [Na^+] [13] and is expected to be useful for diagnosis of many acute and chronic renal diseases [10], [14, 15]. Applications of ^{23}Na MRI could be applied in cardiac imaging to evaluate the elevation of myocardial TSC in acute ischemia models [16–18] and its potential has been explored in human hearts on 7T [17]. Role of ^{23}Na MRI in oncology to monitor therapy in cancer treatments beyond abdomen is invaluable to detect and quantity changes in TSC at baselines and multiple post chemotherapy images [16]. A robust quantitative ^{23}Na MRI technique with TSC measurements can also be very useful in understanding malignant brain and breast tumors where it has been found that there is an increase in TSC relative to contra-lateral tissues in the brain [19] and non-involved glandular tissue and benign lesions in the breast [20, 21]. ^{23}Na MRI has an emerging application in the brain in terms of stroke management where TSC could be used as a measure of tissue viability and can be used in a complimentary role with diffusion and perfusion in evaluating the ischemia [22]. Applications of ^{23}Na MRI can be extended into human skeletal muscle imaging with potential use in exercise and disease with sodium quantification which will greatly help in understanding the role of Na^+/K^+ pump and perfusion in normal and diseased muscle [23]. A more recent application of ^{23}Na MRI has been in the field of evaluating tumor viability in lung cancers and was proved with direct comparisons with ^{1}H MR, CT, and FDG-PET-CT imaging that this advanced MRI technique could be highly valuable in providing functional molecular information regarding tumor viability [24]. A multimodality approach of combining ^{23}Na MRI with Diffusion-Weighted Imaging (DWI) and ^{1}H MR in uterine

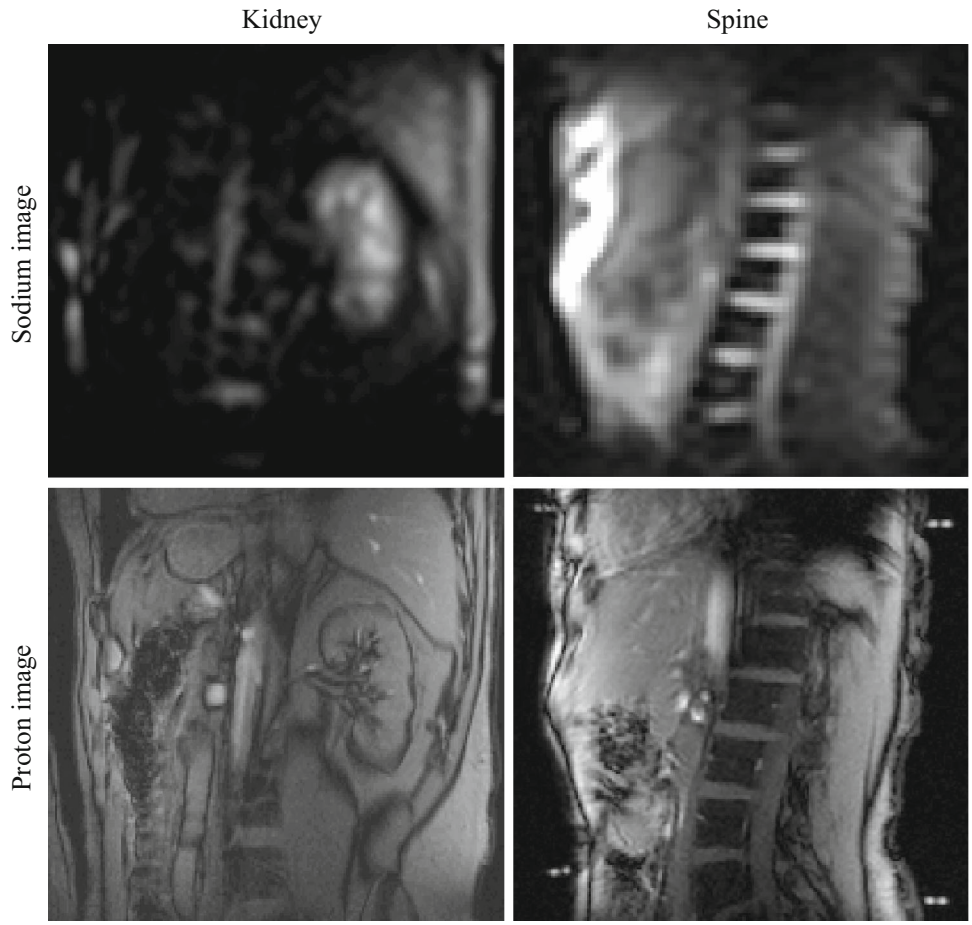

Fig. 6. Representative oblique ^{23}Na and ^{1}H MR slices showing the medullary pyramids in the kidney (*left*) and the intervertebral disks in the spinal cord (*right*).

leiomyomata after MR-guided high-intensity focused ultrasound revealed the potential to explore the molecular and metabolic pathways after treatment [25] with this novel clinical MR technique.

Obtaining in vivo ^{23}Na images and quantifying TSC of the abdomen at 3T using the 8-channel ^{23}Na/^{1}H coil is shown to be feasible and reproducible. The images presented in this work were acquired in less than 15 minutes, an acceptable clinical acquisition time. The images acquired have a reasonably good in-plane resolution and SNR considering that the ^{23}Na signal in tissue is ~10^{-4} times weaker than the water ^{1}H signal. The SNR reported in this work for abdominal imaging is slightly lower than the literature reported SNR of ~36 for volume type bird cage sodium coils developed for knee and brain imaging applications but considering that the coil presented in this work is a surface-type phased-array coil, the SNR is optimal and adequate for abdominal sodium imaging and has SNR comparable to abdominal sodium work presented by Steidle et al. [26]. The in-plane resolution achieved with this coil (0.3 x 0.3 cm^2) is also comparable to the reported values [27, 28]

The whole volume ^{23}Na imaging protocol developed in this study facilitated for a better coverage and for shorter imaging time, since it aided in reducing the TE considerably by allowing the use of a non-selective RF excitation pulse. 3D imaging of the whole volume was employed for better coverage and for shorter imaging time since it aided in reducing the TE considerably by allowing the use of a non-selective RF excitation pulse. The sequence used for ^{23}Na imaging in our study is a spoiled 3D GE sequence, commonly known as VIBE sequence. VIBE stands for Volumetric Interpolated Breath Hold Examination developed by Rofsky et al. [8]. VIBE is a commonly used sequence for abdominal MR imaging. This sequence is used for achieving short acquisition times and resolution improvements through the use of asymmetric k-space sampling and interpolation. Typically asymmetric echoes with volumetric sampling help in reducing the number of phase encoding steps and reduces the overall imaging time. The loss in the SNR due to the reduction in the imaging time can be compensated by increasing the number of signal averages. The changes made to optimize the vendor-provided 3D

GRE ^{1}H MRI pulse sequence for ^{23}Na MRI included the use of an asymmetric k-space sampling combined with volumetric interpolation, use of minimum allowed receiver BW, a flip angle that matched the Ernst angle condition and a short TR with large number of signal averages to compensate for signal decay due to short T_1 recovery time for ^{23}Na. These optimizations allowed us to obtain ^{23}Na images with a maximum SNR. Partial Fourier technique aided in reducing scan time from 30 min to ~15 min, but did result in lower resolution images (thickness of 20 mm) and image blurring, but elliptical scanning and the 128 number of averages assisted in gaining the SNR back. Parallel imaging was used to obtain spatial information from the multi-channel phased-array coils which also helped in reducing the number of signal averages needed for a given spatial resolution and aided in reducing the scan time and/or helped in further improving the quality of the sodium images.

Although the efficient coil design with eight receive elements allowed us to image a large torso region in all directions with optimum SNR, a significant B_1 inhomogeneity was observed in the images because the sensitivity of a coil decreased as a function of distance from the coil elements unlike homogenous B_1 distribution for volume coils. There was an exponential drop in the signal intensity toward the center of the image which made the central liver region appear darker. We overcame this significant artifact by creating 3D B_1 calibration maps. The non-corrected acquired ^{23}Na images were then divided with the calibration map on a slice by slice basis to obtain a corrected ^{23}Na image. Exponential curve fit and spherical harmonics were used to create the calibration maps. Higher order spherical harmonics produced more homogeneous ^{23}Na images as seen in Fig. 5.

Various ^{1}H MRI techniques, like diffusion-weighted (DW) imaging, fat-water imaging, etc., are excellent non-invasive techniques to quantitatively image the liver. However, it remains a challenge to distinguish between different pathological conditions of the liver such as hepatitis/cirrhosis. The total sodium quantification through ^{23}Na MRI could be used as another biomarker that could assess liver diseases and monitor the efficiency of treatments with a better understanding of the physiology affecting the sodium concentration. It is our hypothesis that this could be useful for developing a more accurate diagnosis for hepatitis and cirrhosis. An evaluation of the reproducibility and reliability of the liver TSC values showed that TSC values are highly reproducible with only ~4 % variability and not affected significantly by respiratory motion or other hardware factors. The technique used here for evaluating liver tissue sodium concentration can easily be expanded to other organs such as kidneys, pancreas, etc. The measurements of TSC values in this study were computed using the optimally attained long TE (lowest achievable) at 2.8 ms and a short TR of 12 ms. Theoretically other studies use ultra-short TE (sub-milliseconds) and a TR of about 120–200 ms which is more ideal. The reason for keeping a short TR allowable for sodium imaging was due to the study constraints for having an acceptable scan time. The equation used for TSC calculation accounted for T_2 corrections both from $T_{2\text{fast}}$ component (16% contribution) and from the $T_{2\text{slow}}$ component (84% contribution) and the fast relaxation component of 0.16, with corrections for the T1 and T2* effects obtained from Bansal et al.'s work [9]. The TSC values would have smaller deviations from the actual concentration if the bi-exponential relaxation factors were obtained from the saline reference and the human liver images obtained from this study.

We would like to highlight that the ^{23}Na MRI is an excellent complimentary technique to DW MRI to diagnose and monitor pathological conditions [29]. In particular, quantitative ADC values computed from DW images are normally used as biomarkers to identify abnormal tissues for qualitative assessment. However, unlike ^{23}Na MR imaging, ADC values can be significantly different based on the location of the organ being imaged, for example, organs with less motion (brain) and organs with significant motion (liver). Literature reports a wide range of liver ADC values ranging from 1.34×10^{-3} to 1.77×10^{-3} mm^2/s [30, 31]. A separate set of experiments was performed in conjunction with this study to estimate the variability in the ADC values of the liver in a gated and free-breathing DWI sequence. It was found that average liver ADC from the subjects was 1.23 ± 0.07 mm^2/sec with 5.7 % inter-subject variability for gated DW and 1.41 ± 0.16 mm^2/sec with 11.7 % variability for free-breathing DW sequence compared to only 4% with TSC measurements from ^{23}Na images.

While ^{23}Na MRI of the abdomen has mostly remained a research topic, we have shown the feasibility to integrate ^{23}Na MRI into routine clinical practice with a novel multi-channel phased-array coil design and an optimized GRE pulse sequence. The method implemented here addresses several major limitations with the current ^{23}Na technique in translating this to patient imaging. Furthermore, the long acquisition time for ^{23}Na MRI can be significantly reduced with the use of parallel imaging and ultra-short TE. Having only a sample size of three subjects for validation of this 8-channel ^{23}Na/^{1}H coil and technique is a limitation to this study. This study aimed at validating a proof of concept with a novel coil design on healthy volunteers and further studies will be performed to validate this technique in a larger sample of healthy volunteers and patient cohorts with liver and other organ diseases, which has elevated sodium concentration outcomes. Future development will also be aimed at quantifying free and bound sodium using advanced ^{23}Na MRI acquisition techniques.

Conclusion

With the 8-channel $^{23}Na/^{1}H$ coil and optimized imaging parameters, ^{23}Na MRI of the entire torso can be acquired with an in-plane spatial resolution of 0.3 cm and an SNR of ~20 within 15 min at 3T without exceeding the FDA-recommended SAR limit for human imaging. The obtained ^{23}Na images allow clear delineation between different abdominal organs and their sub-regions. A method was also developed to correct for RF inhomogeneity produced by the phased-array coil and to calculate TSC from the corrected ^{23}Na MR images. In addition, the reproducibility of TSC measured from ^{23}Na MRI was evaluated in normal subjects. TSC values from the ^{23}Na MR images are reproducible with insignificant inter- and intra-volunteer variability. The future area of development of ^{23}Na MRI will be focused on implementing and enhancing the ^{23}Na imaging protocols incorporating UTE and parallel imaging and also evaluating the use of the technique for disease diagnosis and monitoring therapy response by quantifying free and bound sodium.

Acknowledgments. This research was supported in part by National Institutes of Health (NIH) grant numbers CA110107 and EB005964. The authors thank Helmut Stark, PhD, (MRI Coils Research, Stark Contrast, Erlangen, Germany) for his assistance with coil design and manufacturing, the volunteers for MRI scans, Ms. S. Dharamadhikari and Ms. B. George for technical assistance, and Dr. Andriy Babsky and Dr. Andrew A Smith (*University of Mississippi Medical Centre*, *Jackson*, *MS*) for their valuable discussion and editorial comments.

References

1. Nogae S, Michimata M, Kanazawa M, et al. (2000) Cardiac infarcts increase sodium transporter transcripts (rBSC1) in the thick ascending limb of Henle. Kidney Int 57(5):2055–2063
2. Ouwerkerk R, Jacobs MA, Macura KJ, et al. (2007) Elevated tissue sodium concentration in malignant breast lesions detected with non-invasive 23Na MRI. Breast Cancer Res Treat 106(2):151–160
3. Madelin G, Regatte RR (2013) Biomedical applications of sodium MRI in vivo. J Magn Reson Imaging 38(3):511–529
4. Romanzetti S, Mirkes CC, Fiege DP, Celik A, Felder J, Shah NJ (2014) Mapping tissue sodium concentration in the human brain: a comparison of MR sequences at 9.4Tesla. Neuroimage 96:44–53
5. Lanz T, Mayer M, Roboson MD, Neubauer S, Ruff J, Weisser A (2007) An 8-channel ^{23}Na heart array for application at 3 T. In: Proceedings in international society of magnetic resonance medicine
6. Panda A, Jones S, Stark H, et al. (2012) Phosphorus liver MRSI at 3 T using a novel dual-tuned eight-channel (3)(1)P/(1)H H coil. Magn Reson Med 68(5):1346–1356
7. American College of Radiology (ACR) (1998) Phantom test guidance for the ACR MRI Accreditation Program. Reston, VA
8. Rofsky NM, Lee VS, Laub G, et al. (1999) Abdominal MR imaging with a volumetric interpolated breath-hold examination. Radiology 212(3):876–884
9. Bansal N, Germann MJ, Seshan V, et al. (1993) Thulium 1,4,7,10-tetraazacyclododecane-1,4,7,10-tetrakis(methylene phosphonate) as a 23Na shift reagent for the in vivo rat liver. Biochemistry 32(21):5638–5643
10. Atthe BK, Babsky AM, Hopewell PN, et al. (2009) Early monitoring of acute tubular necrosis in the rat kidney by 23Na-MRI. Am J Physiol Renal Physiol 297(5):F1288–1298
11. Babsky AM, Topper S, Zhang H, et al. (2008) Evaluation of extra- and intracellular apparent diffusion coefficient of sodium in rat skeletal muscle: effects of prolonged ischemia. Magn Reson Med 59(3):485–491
12. Hopewell PN, Bansal N (2008) Noninvasive evaluation of nonalcoholic fatty liver disease (NAFLD) using ^{1}H and ^{23}Na magnetic resonance imaging and spectroscopy in a rat model. Proc Int Soc Magn Reson Med
13. Nagy IZ, Lustyik G, Nagy VZ, Zarandi B, Bertoni-Freddari C (1981) Intracellular Na^{+}:K^{+} ratios in human cancer cells as revealed by energy dispersive x-ray microanalysis. J Cell Biol 90(3):769–777
14. Rosen Y, Lenkinski RE (2009) Sodium MRI of a human transplanted kidney. Acad Radiol 16(7):886–889
15. Maril N, Rosen Y, Reynolds GH, et al. (2006) Sodium MRI of the human kidney at 3 Tesla. Magn Reson Med 56(6):1229–1234
16. Ouwerkerk R (2007) Sodium magnetic resonance imaging: from research to clinical use. J Am Coll Radiol 4(10):739–741
17. Graessl A, Ruehle A, Renz W, et al. (2013) Sodium imaging of the heart at 7T: design, evaluation and application of a four-channel transmit/receive surface coil array. J Cardiovas Magn Reson 15(Suppl 1):W14–W14
18. Ouwerkerk R, Bottomley PA, Solaiyappan M, et al. (2008) Tissue sodium concentration in myocardial infarction in humans: a quantitative 23Na MR imaging study. Radiology 248(1):88–96
19. Ouwerkerk R, Bleich KB, Gillen JS, Pomper MG, Bottomley PA (2003) Tissue sodium concentration in human brain tumors as measured with 23Na MR imaging. Radiology 227(2):529–537
20. Ouwerkerk R, Jacobs MA, Macura KJ, et al. (2007) Elevated tissue sodium concentration in malignant breast lesions detected with non-invasive 23Na MRI. Breast Cancer Res Treat 106(2):151–160
21. Jacobs MA, Ouwerkerk R, Wolff AC, et al. (2011) Monitoring of neoadjuvant chemotherapy using multiparametric, (2)(3)Na sodium MR, and multimodality (PET/CT/MRI) imaging in locally advanced breast cancer. Breast Cancer Res Treat 128(1):119–126
22. Thulborn KR, Gindin TS, Davis D, Erb P (1999) Comprehensive MR imaging protocol for stroke management: tissue sodium concentration as a measure of tissue viability in nonhuman primate studies and in clinical studies. Radiology 213(1):156–166
23. Constantinides CD, Gillen JS, Boada FE, Pomper MG, Bottomley PA (2000) Human skeletal muscle: sodium MR imaging and quantification-potential applications in exercise and disease. Radiology 216(2):559–568
24. Henzler T, Konstandin S, Schmid-Bindert G, et al. (2012) Imaging of tumor viability in lung cancer: initial results using 23Na-MRI. Rofo 184(4):340–344
25. Jacobs MA, Ouwerkerk R, Kamel I, et al. (2009) Proton, diffusion-weighted imaging, and sodium (23Na) MRI of uterine leiomyomata after MR-guided high-intensity focused ultrasound: a preliminary study. J Magn Reson Imaging 29(3):649–656
26. Steidle G, Graf H, Schick F (2004) Sodium 3-D MRI of the human torso using a volume coil. Magn Reson Imaging 22(2):171–180
27. Wetterling F, Tabbert M, Junge S, et al. (2010) A double-tuned (1)H/(23)Na dual resonator system for tissue sodium concentration measurements in the rat brain via Na-MRI. Phys Med Biol 55(24):7681–7695
28. Kim JH, Moon CH, Park BW, et al. (2012) Multichannel transceiver dual-tuned RF coil for proton/sodium MR imaging of knee cartilage at 3 T. Magn Reson Imaging 30(4):562–571
29. Jacobs MA, Ouwerkerk R, Kamel I, et al. (2009) Proton, diffusion-weighted imaging, and sodium (23Na) MRI of uterine leiomyomata after MR-guided high-intensity focused ultrasound: a preliminary study. J Magn Reson Imaging 29(3):649–656
30. Kilickesmez O, Yirik G, Bayramoglu S, Cimilli T, Aydin S (2008) Non-breath-hold high b-value diffusion-weighted MRI with parallel imaging technique: apparent diffusion coefficient determination in normal abdominal organs. Diagn Interv Radiol 14(2):83–87
31. Miquel ME, Scott AD, Macdougall ND, et al. (1019) In vitro and in vivo repeatability of abdominal diffusion-weighted MRI. Br J Radiol 2012(85):1507–1512